



Zinc Doping Enhances the Electrocatalytic Properties of Cobalt Borides for the Hydrogen Evolution Reaction

Javier Quílez-Bermejo^{1,2*}, Sergio García-Dalí^{1,3}, Raj Karthik¹, Rafael Canevesi¹, María T. Izquierdo⁴, Mélanie Emo⁵, Alain Celzard¹ and Vanessa Fierro^{1*}

¹Centre National de la Recherche Scientifique (CNRS), Institut Jean Lamour (IJL), Université de Lorraine, Épinal, France, ²Departamento de Química Inorgánica and Instituto de Materiales, Universidad de Alicante, Alicante, Spain, ³Departamento de Ciencia de los Materiales e Ingeniería Metalúrgica, Universidad de Oviedo, Oviedo, Spain, ⁴Instituto de Carboquímica (ICB-CSIQ), Zaragoza, Spain, ⁵Centre National de la Recherche Scientifique (CNRS), Institut Jean Lamour (IJL), Université de Lorraine, Nancy, France

OPEN ACCESS

Edited by:

Simona Liguori,
Clarkson University, United States

Reviewed by:

Yongqiang Feng,
Shaanxi University of Science and
Technology, China
Jayeeta Chattopadhyay,
Amity University Jharkhand, India

*Correspondence:

Javier Quílez-Bermejo
javier.quilez-bermejo@univ-lorraine.fr
Vanessa Fierro
vanessa.fierro@univ-lorraine.fr

Specialty section:

This article was submitted to
Hydrogen Storage and Production,
a section of the journal
Frontiers in Energy Research

Received: 21 March 2022

Accepted: 21 April 2022

Published: 12 May 2022

Citation:

Quílez-Bermejo J, García-Dalí S,
Karthik R, Canevesi R, Izquierdo MT,
Emo M, Celzard A and Fierro V (2022)
Zinc Doping Enhances the
Electrocatalytic Properties of Cobalt
Borides for the Hydrogen
Evolution Reaction.
Front. Energy Res. 10:901395.
doi: 10.3389/fenrg.2022.901395

Electrochemical water splitting requires new, low-cost cathode electrodes for the hydrogen evolution reaction to enable the worldwide implementation of electrolyzers. Cobalt borides are proposed as one of the most promising materials to overcome the limitations of the commercial electrocatalysts, but the catalytic activity still needs to be improved to be competitive. Here, we report that the introduction of zinc into cobalt boride to produce a ternary cobalt boride is an efficient route to further improve the catalytic activity towards the hydrogen evolution reaction (HER) of cobalt boride. The ternary Co-Zn-B was prepared by an easy chemical reduction method to achieve superior HER electrocatalytic performance with a lower overpotential than the homologous Co-B. The larger surface area, structural order, crystallization degree and, in particular, the different surface chemistry seem to be key factors for this improvement.

Keywords: Zn doping, cobalt borides, HER, water splitting, electrolyzer

INTRODUCTION

The hydrogen economy is proposed as a viable and efficient strategic model to replace the current economic system based on fossil fuel combustion (Abdin et al., 2020; Fan et al., 2021). The main advantage of hydrogen as an energy vector is its potential to supply energy without any dependence on an external factor, thus overcoming the intermittency of other renewable systems, such as solar and wind power (Abdin et al., 2020; Thomas et al., 2020; Fan et al., 2021; Singla et al., 2021). The impact and relevance of hydrogen in the following years is such that the Hydrogen Roadmap for Europe predicts that it will provide up to 24% of total energy demand in the European Union by 2050 (Hydrogen Roadmap Europe, 2019). However, the hydrogen economic system in the new economic forecasts will only be viable if hydrogen is obtained from renewable technologies (known as green hydrogen).

The most promising strategy to produce green hydrogen is electrochemical water splitting, which is the most efficient route to produce hydrogen with zero-net carbon emissions (Wang et al., 2020; Zhou and Fan, 2021). Water electrolysis requires the use of expensive electrocatalysts in the cathode electrode for solving the sluggish kinetics of the hydrogen evolution reaction (HER) (Murthy et al., 2018; Yu et al., 2019; Wu et al., 2021). Nevertheless, the most efficient electrocatalysts are based on

platinum nanoparticles supported on carbon black. Platinum is a rare material in nature, makes the cost of these electrocatalysts unaffordable to enable the worldwide implementation of electrolyzers. Different alternatives to platinum-based catalysts have been proposed in recent years and can be classified into two groups: (i) metal-free carbon-based electrocatalysts (Hu and Dai, 2016; Murthy et al., 2018; Nemiwal et al., 2021) and (ii) non-precious metal-based electrocatalysts (Siwal et al., 2020; Zhou et al., 2020). The latter have attracted the attention of the scientific community because of the low cost of these metals and the easy preparation of the electrocatalysts while retaining most of the chemical features of metal nanoparticles.

Transition metal borides (TMBs) have attracted considerable attention in recent years due to their excellent electrocatalytic properties for HER (Gupta et al., 2020; Pu et al., 2021; Yao et al., 2021). However, most of the TMBs exhibit poor catalytic performance in alkaline water electrolysis. Cobalt boride (Co-B) is the most promising HER electrocatalyst among all TMBs since it is considered a robust, stable and efficient catalyst as cathode electrode for electrochemical water splitting (Gupta et al., 2015; Masa et al., 2016; Chen et al., 2018). Recent works have attempted to enhance the electrocatalytic performance of Co-B by introducing a second metal in the pristine Co-B structure such as Fe (Qiang et al., 2021), Ni (Xu et al., 2017; Dutta et al., 2020) and others (Fernandes et al., 2020). However, to the best of our knowledge, the introduction of Zn and the impact in the physicochemical and electrochemical properties of the resulting Zn doped Co-B has not yet been studied.

Inspired by the high catalytic activity of Co-B, we report a simple and effective strategy for the preparation of improved HER electrocatalysts based on ternary metal boride doped with Zn (Co-Zn-B) through a well-known chemical reduction method (Tan et al., 2019). The resulting Co-Zn-B catalysts were extensively characterized by XRD, XPS, N₂-adsorption isotherms, TEM, EDS and electrochemical characterization. These new catalysts led to an improved HER performance with significantly enhanced kinetics compared to the pristine Co-B, postulating the doping of Zn in TMBs as a new opportunity to improve the properties of metal borides for multiple applications.

MATERIALS AND METHODS

Preparation of Co-Zn-B

A ternary metal boride based on Co and Zn (Co-Zn-B) was prepared through a chemical reduction method by combining different metals precursors in the synthesis. 50 ml of a 0.1 M aqueous solution of the Zn precursor, Zn(NO₃)₂, was added into 50 ml of the Co precursor, a 0.3 M aqueous solution of CoCl₂. After vigorous stirring to ensure adequate contact of all precursors, 15 ml of 0.3 M NaBH₄ was added to the mixture. The resulting solution was then stirred for 30 min until a powder was obtained. The resulting material is filtered and washed with water. The generated powder was introduced into a tubular furnace for further heat treatment in N₂ atmosphere with a heating rate of 1°C min⁻¹ up to 350°C and this temperature

was maintained for 2 h. Prior to the heat treatment, the furnace was purged with a N₂ flow of 150 ml min⁻¹. The same flow was kept during the heat treatment. The same procedure was employed for the preparation of Co-B material, but without the addition of the Zn precursor.

Figure 1 illustrates the experimental method for the preparation of Co-B and Co-Zn-B.

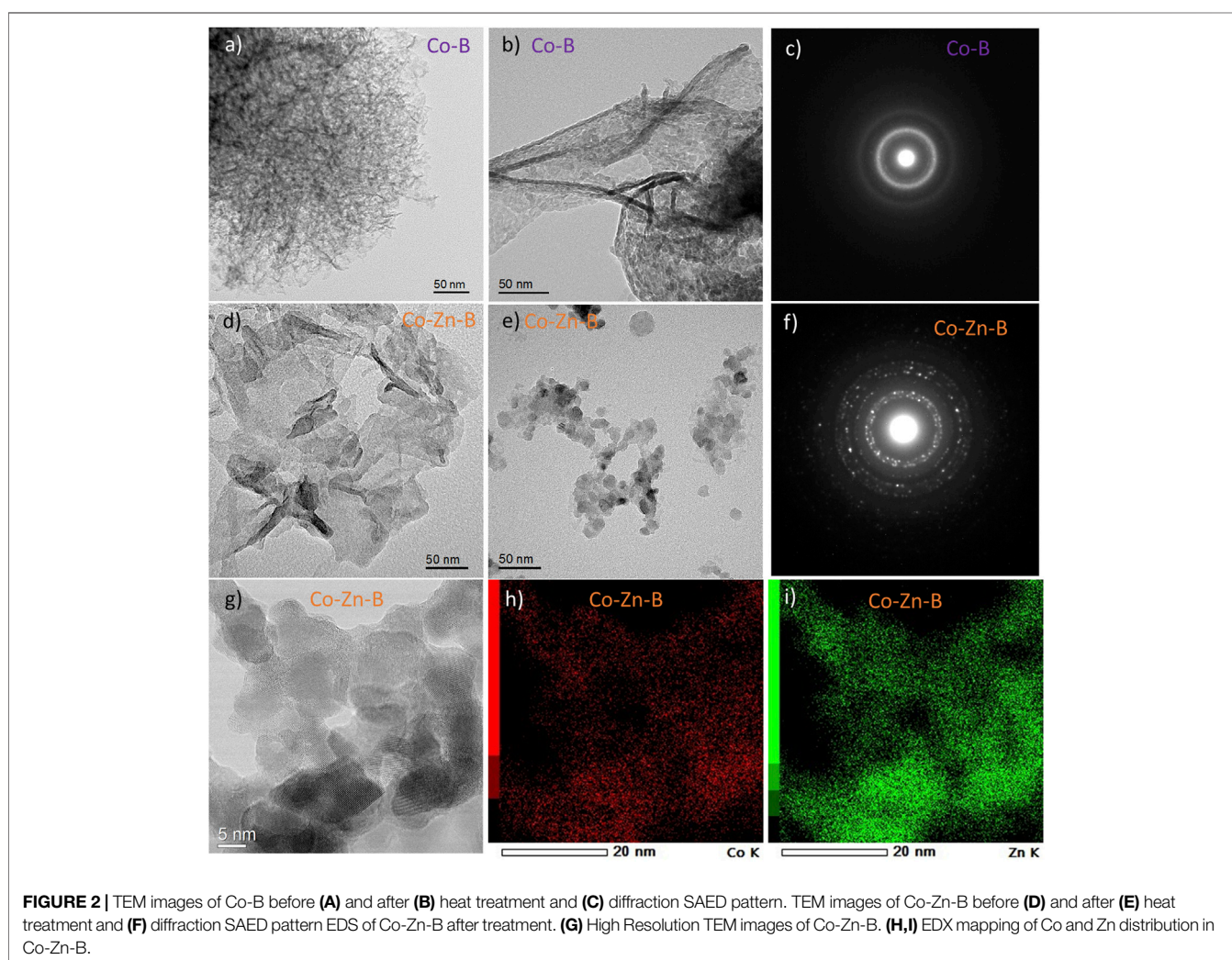
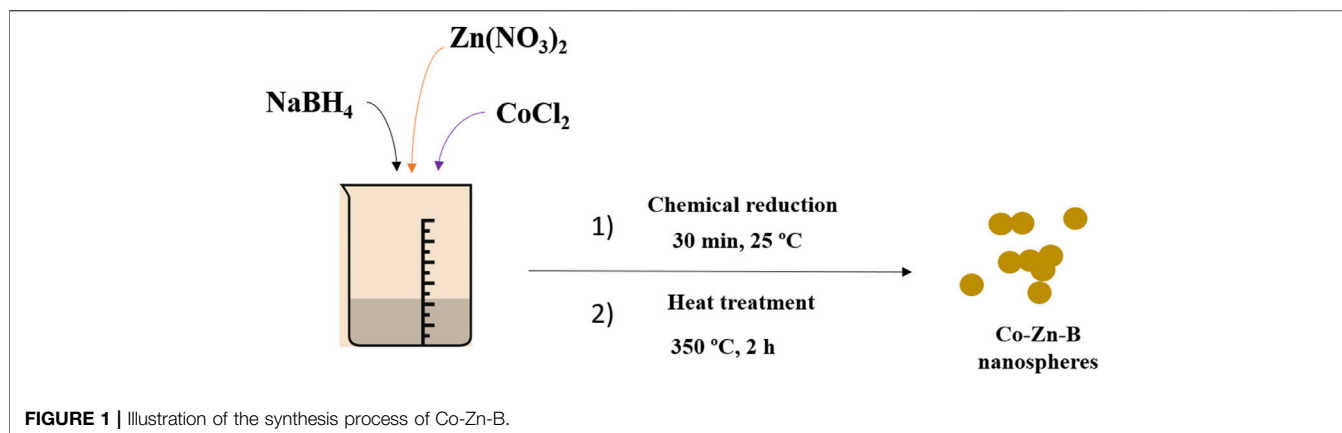
Physicochemical Characterization

Transmission electron microscopy (TEM) images were acquired by a JEM—ARN 200 F Cold FEC TEM/STEM equipped with a probe and image spherical aberration correctors. Prior to the experiments, the samples were prepared by dispersing the powdered working material in an ethanol solution via sonication. Once the suspension was obtained, the material was drop-cast and deposited on a carbon-coated TEM grid (200 mesh) and dried under ambient conditions. Particle size distribution of the samples was measured by laser diffraction using a Mastersizer 3000 (Malvern Panalytical) analyzer. Prior to the measurements, the powder was dispersed in distilled water.

The crystallization degree and structural order of the samples were studied through X-ray Powder Diffraction (XRD) using a Bruker D8 Advance A25 polycrystalline powder X-ray diffractometer. Textural properties, BET areas (A_{BET}) among them (Brunauer et al., 1938), were obtained from N₂ adsorption isotherms performed at -196°C on a fully automatized ASAP2020 manometric adsorption unit (Micromeritics, Atlanta, GA). Prior to the measurements, the samples were degassed under high vacuum (1.0 × 10⁻³ Pa) and 110°C for 24 h (Jagiello et al., 2021). X-ray photoelectron spectroscopy (XPS) was obtained by using an ESCAplus OMICROM spectrometer equipped with a non-monochromatized MgKα X-ray source. Shirley-type background and quantification were processed using the CASA software. Peak deconvolution was performed by XPSPEAK software using 20:80 Laurentizan:Gaussian fitting.

Electrochemical Characterization

The electrochemical characterization of Co-B and Co-Zn-B was studied in a conventional three-electrode cell equipped with a rotating ring-disk electrode (RRDE) in a PGSTAT302N bi-potentiostat (Metrohm). The working electrode was prepared as detailed elsewhere (Bouleau et al., 2022). Briefly, the working electrode consists of a glassy carbon disk of 0.196 cm² and a second working electrode based on a platinum ring surrounding the working carbon-based electrode. To prepare the working electrode, the Co-Zn-B and Co-B powdered samples were suspended in a concentration of 4 mg ml⁻¹ in a 20% aqueous isopropanol solution with a 0.2 wt% Nafion®. A total of 33.68 μL of the suspension were drop-casted into the working electrode to obtain a carbon loading of 0.7 mg cm². The material was dried under an IR lamp at approximately 80°C. Then, the electrode is introduced in the working electrolyte under vacuum conditions for few minutes to ensure adequate wettability of the electrodes (Bouleau et al., 2022). A reversible hydrogen electrode was used as the reference electrode and a glassy carbon rod of 8 mm in diameter was used as the counter electrode. The RHE consists of a platinum electrode, which is immersed in the working



electrolyte. After applying a voltage, pure hydrogen is produced at the reference electrode and can be used for the electrochemical measurements. The stability of the RHE was checked and confirmed before the measurements.

The electrochemical behavior was analyzed through cyclic voltammetries (CV) in a N_2 -saturated 1.0 M KOH solution at 50 mV s^{-1} . The electrocatalytic activity towards HER was studied by linear sweep voltammetry (LSV) in a N_2 -saturated 1.0 M KOH

solution between 0.2 and -1.0 V vs. RHE at 1,600 rpm and a scan rate of 5 mV s^{-1} . Tafel slopes were obtained from the linear fitting of the $\log(j)$ versus the applied potential.

RESULTS AND DISCUSSION

Bright Field TEM images were obtained before and after the heat treatment step. **Figure 2A** shows the TEM image of the undoped Co-B sample before the heat treatment, in which a laminar arrangement was observed. After the heat treatment (**Figure 2B**), the morphology of Co-B material is significantly affected, leading to the formation of small nanospheres of about 10 nm in diameter with a high degree of agglomeration, similar to other cobalt borides in the literature (Chundurri et al., 2019). At the same time, the ternary metal boride (Co-Zn-B) before the heat treatment step shows a high degree of agglomeration degree of thin layers (**Figure 2D**). The heat treatment at 350°C of Co-Zn-B leads to the formation of larger nanospheres of about 25 nm with a lower degree of agglomeration compared to Co-B (**Figure 2E**). Interesting differences were also observed in the diffraction pattern from TEM images of the samples obtained after the heat treatment step. The Co-B diffraction pattern shows that the material is disordered since intense dots are not observed by selected area electron diffraction (SAED), **Figure 2C**. This is characteristic of amorphous phases of cobalt borides (Li et al., 2002; Jiang et al., 2020). At the same time, the sample obtained by adding Zn shows a well-ordered SAED pattern (**Figure 2F**), highlighting the differences in the structural order of both samples. The standard value of 0.1983 nm for (211) plane in cobalt borides confirmed the formation of structured cobalt boride phases (Zhang et al., 2020); however, the major ring contributions are found at standard values of 0.2520 and 0.2832 nm, which are associated with (100) and (002) planes of zinc oxide phases, respectively (Emil et al., 2018). Moreover, **Figure 2G** shows the high-resolution TEM (HRTEM) images of the Co-Zn-B sample, in which a clear atomic order was observed, which confirm the presence of crystalline phases.

Energy Dispersive X-ray Spectroscopy (EDS) was used to obtain information about the chemical nature of the Co-B and Co-Zn-B samples. As observed in **Supplementary Figure S1A**, the EDS profiles show the presence of cobalt, oxygen and boron in the Co-B sample. If the material is prepared with the addition of $\text{Zn}(\text{NO}_3)_2$, a new intense peak is observed in the EDS profile (**Supplementary Figure S1B**), which is attributed to the presence of Zn in the material composition. Moreover, EDS mapping was performed to further check the distribution of Co and Zn atoms in HRTEM images. **Figures 2H,I** show a homogenous distribution of both Co and Zn atoms in Co-Zn-B sample. This confirms the successful doping of Co-B with the presence of Zn in the bulk. In addition, the presence of small traces of Cl was detected in Co-Zn-B sample, probably originating from the CoCl_2 used in the synthesis (**Figure 2F**). It is interesting to note that this Cl peak is not found in the Co-B sample, so only if the Zn is used in the synthesis the Cl remains after the heat treatment. This fact suggests that Zn interacts strongly with the chlorides and that, consequently, the Zn-Cl bonds formed are stable after

the 350°C heat treatment in good agreement with previous studies (Jones et al., 2013).

The particle size distributions of the two samples are shown in **Supplementary Figure S2**. The pristine Co-B shows a large and broad contribution centered at $43 \mu\text{m}$, with a minor contribution at $10 \mu\text{m}$. At the same time, the sample obtained with the introduction of Zn (Co-Zn-B) led to a significant decrease in particle size to a unimodal peak centered at about $17 \mu\text{m}$. The crystallization degree and the structural order of Co-B and Co-Zn-B were studied via X-ray diffraction (XRD). The XRD-profile of Co-B (**Figure 3A**) shows the predominance of a disordered cobalt boride structure (PDF 75-1066), as shown by the broad peak at 44.5° , characteristic of amorphous domains of cobalt boride phase (green triangle in **Figure 3A**) (Wang et al., 2004). In addition, the broad peaks at 37° indicate the presence of CoO (PDF-721474) and Co_3O_4 (PDF-65-3103) cobalt oxide phases (blue circle in **Figure 3A**). This means that our Co-B sample does not only consist of cobalt boride domains, but there is also the presence of cobalt oxides in its composition. On the other hand, the XRD-profile of Co-Zn-B sample (**Figure 3A**) is significantly different compared to Co-B sample, since a clear structural order is observed, as confirmed in the diffraction pattern from TEM images. Multiple peaks related to zinc oxide (PDF-653411) (black squares in **Figure 3A**) and zinc chloride (PDF-070155) (red squares in **Figure 3A**) are defined, showing that most of the order originates from the metal oxide phases. The presence of zinc chloride peak confirmed what was suggested in the EDS profile, the presence of Zn-Cl phases. The peak related to metal borides phase (green triangle in **Figure 3A**) is slightly observed at 44.5° , which indicates that this phase is present in the form of amorphous domains, as in Co-B sample.

The surface chemistry of the samples was studied by X-ray photoelectron spectroscopy (XPS) and the quantification of the different elements in the two cobalt borides are gathered in **Table 1**. The amount of Co in the composition decrease from 16.2 at.% to 7.4 at.% after the addition of Zn in the synthesis of the samples. This decrease in the Co amount is related to the introduction of Zn atoms into the structure of the cobalt boride, which was found to be 7.6 at.% in Co-Zn-B. The total metal amount in the ternary metal borides was 15.0 at.%, which is similar to that in pristine Co-B. This means that the Zn atoms are introduced in substitution of the Co atoms in the structure, maintaining similar metal content in the borides. Moreover, **Table 1** also shows that the O and B contents are similar for both samples, indicating that the only differences in the surface chemistry of these samples are found in the metal composition.

The individual deconvolution of the Co $2p_{3/2}$ reveals important information about the effect of the Zn in the pristine Co-B structure. **Figure 3B** shows the Co $2p_{3/2}$ profile of Co-B, in which two main peaks were detected. The first peak at $780.7 \pm 0.2 \text{ eV}$ is related to the presence of Co^{3+} and the second peak at $782.7 \pm 0.2 \text{ eV}$ is associated with Co^{2+} (Tan et al., 2019; Wang et al., 2021). In addition, the satellite peak is located at $785\text{--}787 \text{ eV}$. In the case of Co-B material, the ratio $\text{Co}^{3+}/\text{Co}^{2+}$ is about 1.6, which indicates the larger contribution of Co^{3+} on the electrocatalysts surface. However, if Zn is introduced in the synthesis of cobalt borides, the Co^{3+} contribution increases to

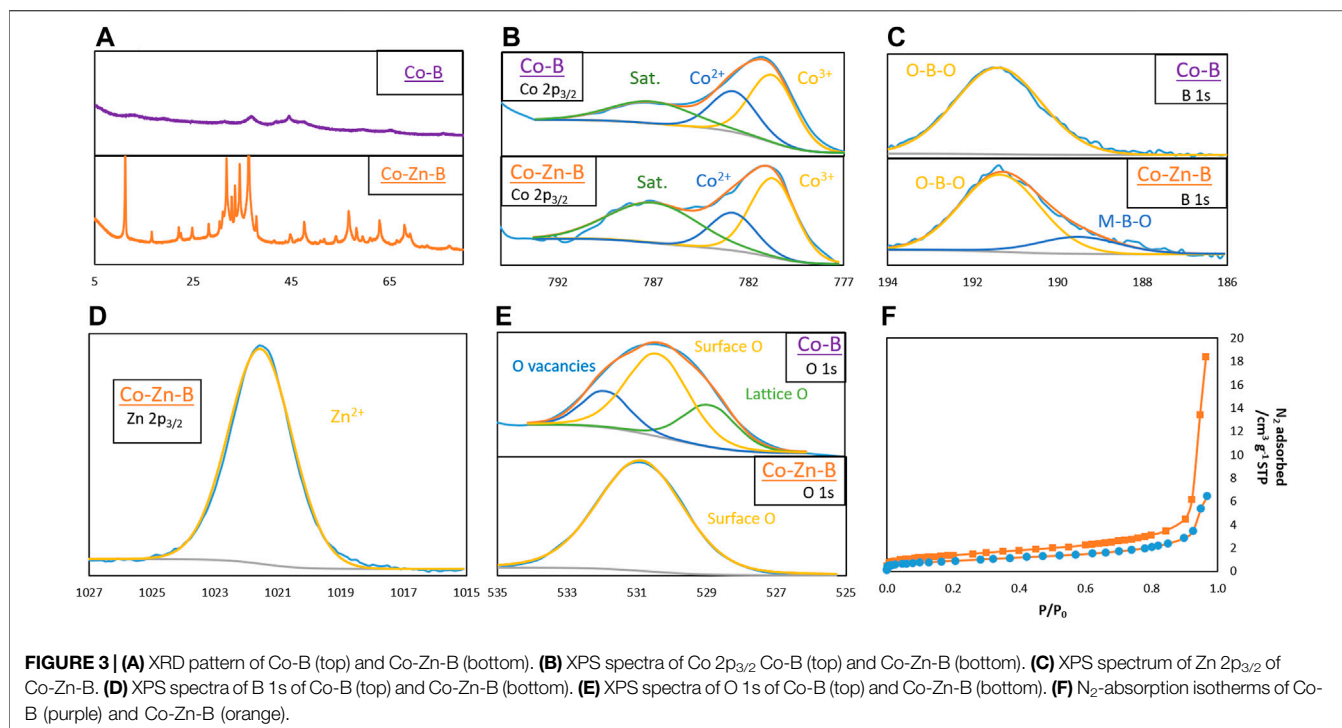


FIGURE 3 | (A) XRD pattern of Co-B (top) and Co-Zn-B (bottom). (B) XPS spectra of Co 2p_{3/2} of Co-B (top) and Co-Zn-B (bottom). (C) XPS spectrum of Zn 2p_{3/2} of Co-Zn-B. (D) XPS spectra of B 1s of Co-B (top) and Co-Zn-B (bottom). (E) XPS spectra of O 1s of Co-B (top) and Co-Zn-B (bottom). (F) N₂-adsorption isotherms of Co-B (purple) and Co-Zn-B (orange).

TABLE 1 | Atomic percentage of cobalt (Co), oxygen (O), boron (B) and zinc (Zn), Metal/Cobalt (M/Co) and Co³⁺/Co²⁺ ratios, obtained by XPS, and area BET (A_{BET}), obtained from N₂-adsorption isotherms.

Sample	Co (at.%)	Co ³⁺ /Co ²⁺ ratio	Zn (at.%)	Zn/Co ratio	O (at.%)	B (at.%)	A _{BET} (m ² /g)
Co-B	16.2	1.6	-	-	56.5	27.3	70
Co-Zn-B	7.4	2.1	7.6	1.0	53.9	31.0	112

a Co³⁺/Co²⁺ ratio of 2.1. This indicates that chemical changes in the morphology and structural order are accompanied by a higher oxidation state of the cobalt atoms in the cobalt boride structure. On the other hand, the Zn 2p_{3/2} profile of Co-Zn-B (Figure 3C) shows the presence of single peak at 1,021.8 eV, which is related to the presence of Zn²⁺ according to the literature (Choi et al., 2016; Liang and Wang, 2018).

B 1s was studied to understand the chemical changes associated with the boron element. Figure 3D shows the B 1s profiles of Co-B and Co-Zn-B samples. The peak at 191.6 eV, which is related to the presence of O-B-O (Sun et al., 2019; Sukanya and Chen, 2020; Zhao et al., 2022), is observed in both profiles, however, a new peak appears at 189.4 eV after the introduction of the Zn into the cobalt boride composition. This peak is related to the contribution of M-B-O moieties, which reveals the formation of metal boride species (Sun et al., 2019; Sukanya and Chen, 2020; Zhao et al., 2022). In the case of the oxygen moieties, the O 1s spectra of the two samples were evaluated and Figure 3E shows the O 1s profiles. The pristine material shows the contribution of lattice O (at 529.1 eV), surface O groups (at 530.6 eV) and O vacancies (at 532.1 eV) (Wu et al., 2015; Masa et al., 2016). However, the addition of Zn results in the disappearance of the both lattice O

and O vacancies. Thus, Co-Zn-B only shows the contribution of surface O in the composition.

Figure 3F shows the N₂ adsorption isotherms of both samples and Table 1 summarizes the most important data. The undoped Co-B material has an A_{BET} of 70 m² g⁻¹, typical of cobalt borides. However, when the Zn-based ternary metal boride is formed, the A_{BET} increases up to 112 m² g⁻¹. The significant changes in the morphology and the structural order seem to have a direct impact on the textural properties of the cobalt borides, leading to an increase of more than 30% in the apparent surface area.

Figure 4A shows the CVs of both samples in a N₂-saturated 1.0 M KOH solution at 50 mV s⁻¹. The pristine Co-B material shows a CV-profile similar to that of cobalt borides in the literature (Li et al., 2020). As observed in Figure 4A, the CV-profile of the sample modified with Zn does not present significant differences, but only a slight tilt was observed, probably due to a lower electrical conductivity of the material. The CV-profile of Co-Zn-B shows a similar behavior to that observed for Co-B, which means that the double layer capacitance is similar between the two samples (23.4 and 28.0 mF g⁻¹ for Co-B and Co-Zn-B, respectively). This slightly higher capacitance value for Co-Zn-B can be clearly associated with the larger A_{BET} of this sample (see Table 1), resulting in a larger surface area accessible to the electrolyte.

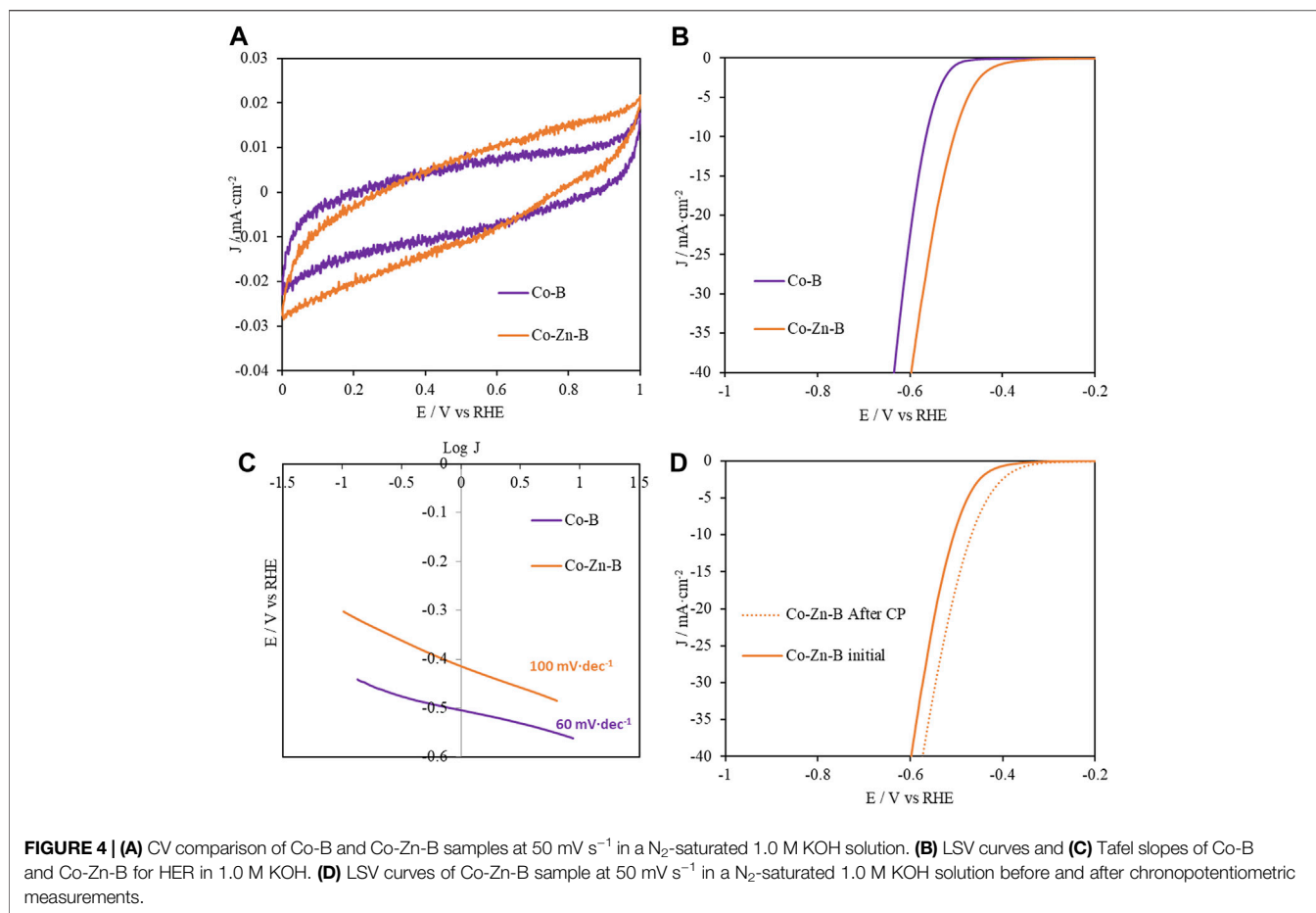


Figure 4B shows the LSV curves for all samples at 1,600 rpm and 5 mV s⁻¹ in a N₂-saturated 1.0 M KOH solution. The LSV curve of Co-B shows a poor catalytic performance towards the HER, with an E_{HER} of -0.57 V vs. RHE (overpotential = 570 mV), which is far from the commercial platinum-like performance, about -0.1 V, or state-of-the-art HER electrocatalysts (Feng et al., 2021; Feng Y et al., 2022; Feng W et al., 2022). However, significant changes in the morphology, structural order and surface chemistry also resulted in an important change in the catalytic activity towards the HER. The Co-Zn-B material shows a significant increase of the catalytic activity, with an E_{HER} of -0.50 V vs. RHE (overpotential = 500 mV). Although this result is still far from the commercial electrocatalysts, it suggests that the introduction of Zn induces significant changes in the electron density of the material, which also leads to an improvement in electrocatalytic activity. Interestingly, this change in the HER activity is not accompanied by a different electrochemical active surface area (ECSA), as shown in **Figure 4A**, which means that the different catalytic activity towards the HER comes from the changes in the physicochemical properties obtained by the introduction of Zn. This is also confirmed in the Tafel slopes, which provide information about the kinetics of both electrocatalysts for the HER. **Figure 4C** shows the Tafel plots of Co-B and Co-Zn-B samples. The pristine material shows a low Tafel slope of 60 mV dec⁻¹, which is characteristic of materials in which the Heyrovsky

stage (M-H_{ads} + H⁺ + e⁻ ↔ H₂ + M) is the rate-determining stage of the hydrogen evolution mechanism (Fang and Liu, 2014). Meanwhile, the ternary metal boride shows a higher Tafel slope of 100 mV dec⁻¹, significantly different from that obtained by the Co-B material. Tafel slopes close to 120 mV dec⁻¹ indicate that the rate-determining stage in the HER is the Volmer stage, which is associated with the adsorption of the hydrogen atoms on the surface of the electrocatalysts (M + H⁺ + e⁻ ↔ M-H_{ads}) (Fang and Liu, 2014). This reveals that the HER on the Co-B and Co-Zn-B sample does not proceed through the same mechanism and this can only be explained if the active sites are different in the two samples since the HER mechanisms are limited by different rate-determining stages. The incorporation of Zn in the structure of Co-B leads to the formation of new active sites that reduce oxygen molecules more efficiently than the pristine Co-B. Therefore, the contribution of a larger surface area, a larger contribution of the Co³⁺ oxidation state or a higher structural order after the introduction of Zn resulted in a better HER catalytic activity in cobalt borides.

To assess whether the HER performance damaged the chemical nature of the Co-Zn-B material, CV before and after the HER measurements were performed. **Supplementary Figure S3** shows that the CV-profile does not exhibit any significant change in the electrochemical behavior of Co-Zn-B, suggesting strong stability under HER working conditions. Furthermore, to confirm the high stability

of the Co-Zn-B sample, chronopotentiometric (CP) measurements were performed at a fixed current density of -5 mA cm^{-2} (Supplementary Figure S4). Figure 4D shows the LSV curves before and after the CP measurements of the most catalytic sample. As observed, there is a slight improvement of the electrocatalytic activity towards the HER after CP measurements, probably related to better electrode wettability after the working conditions. This demonstrates that the introduction of Zn into the Co-B structure leads to the preparation of a robust and stable HER electrocatalysts with improved catalytic activity compared to the pristine Co-B. This study should be considered as preliminary work and a proof of concept and ongoing studies are being done on the addition of different amounts of Zn.

CONCLUSION

A ternary Co-Zn-B boride was successfully prepared by using a simple chemical reduction method of the metal precursors by sodium borohydride. The introduction of Zn into cobalt boride (Co-B) by this method leads to a 7.6 at.% content, which induces significant changes in multiples features of the pristine Co-B, such as larger surface area, higher structural order and higher crystallization degree as well as a shift of the particle size distribution towards a smaller size. Nevertheless, the electrochemical characterization of the Co-Zn-B and Co-B sample, does not show significant differences in the CV-profiles, suggesting similar electrochemical behavior. Nonetheless, the Co-Zn-B material exhibits better electrocatalytic activity towards the hydrogen evolution reaction (HER) compared to Co-B. The electrocatalytic experiments and Tafel slopes suggest that different active sites were created with the introduction of Zn since different HER kinetics and mechanisms were detected. In this study, the introduction of Zn proved to be a useful strategy to modify the chemical and electrochemical properties of Co-B, which may be useful not only for HER but also for other applications.

REFERENCES

- Abdin, Z., Zafaranloo, A., Rafiee, A., Mérida, W., Lipiński, W., and Khalilpour, K. R. (2020). Hydrogen as an Energy Vector. *Renew. Sustain. Energy Rev.* 120, 109620. doi:10.1016/j.rser.2019.109620
- Bouleau, L., Pérez-Rodríguez, S., Quílez-Bermejo, J., Izquierdo, M. T., Xu, F., Fierro, V., et al. (2022). Best Practices for ORR Performance Evaluation of Metal-free Porous Carbon Electrocatalysts. *Carbon* 189, 349–361. doi:10.1016/j.carbon.2021.12.078
- Brunauer, S., Emmett, P. H., and Teller, E. (1938). Adsorption of Gases in Multimolecular Layers. *J. Am. Chem. Soc.* 60, 309–319. doi:10.1021/ja01269a023
- Chen, Z., Kang, Q., Cao, G., Xu, N., Dai, H., and Wang, P. (2018). Study of Cobalt Boride-Derived Electrocatalysts for Overall Water Splitting. *Int. J. Hydrogen Energy* 43, 6076–6087. doi:10.1016/j.ijhydene.2018.01.161
- Choi, Y. I., Lee, S., Kim, S. K., Kim, Y.-I., Cho, D. W., Khan, M. M., et al. (2016). Fabrication of ZnO, ZnS, Ag-ZnS, and Au-ZnS Microspheres for Photocatalytic Activities, CO Oxidation and 2-hydroxyterephthalic Acid Synthesis. *J. Alloys Compd.* 675, 46–56. doi:10.1016/j.jallcom.2016.03.070
- Chundurri, A., Gupta, S., Bapat, O., Bhide, A., Fernandes, R., Patel, M. K., et al. (2019). A Unique Amorphous Cobalt-Phosphide-Boride Bifunctional

DATA AVAILABILITY STATEMENT

The raw data supporting the conclusion of this article will be made available by the authors, without undue reservation.

AUTHOR CONTRIBUTIONS

JQ-B and SG-D performed investigation, formal analysis and first draft writing; RK, RC, MI and ME performed investigation and formal analysis; AC performed supervision and writing—review and editing; VF performed conceptualization, supervision, funding acquisition and writing—review and editing.

FUNDING

This study was partly supported by the French PIA project “Lorraine Université d’Excellence,” reference ANR-15-IDEX-04-LUE and the TALISMAN project funded by ERDF (2019-000214).

ACKNOWLEDGMENTS

JQ-B thanks the Ministerio de Universidades, the European Union and the University of Alicante for the financial support (MARSALAS21-21). SG-D thanks the Ministerio de Universidades, the European Union and the University of Oviedo for the financial support (MU-21-UP2021-03030267158).

SUPPLEMENTARY MATERIAL

The Supplementary Material for this article can be found online at: <https://www.frontiersin.org/articles/10.3389/fenrg.2022.901395/full#supplementary-material>

- Electrocatalyst for Enhanced Alkaline Water-Splitting. *Appl. Catal. B Environ.* 259, 118051. doi:10.1016/j.apcatb.2019.118051
- Dutta, S., Han, H., Je, M., Choi, H., Kwon, J., Park, K., et al. (2020). Chemical and Structural Engineering of Transition Metal Boride towards Excellent and Sustainable Hydrogen Evolution Reaction. *Nano Energy* 67, 104245. doi:10.1016/j.nanoen.2019.104245
- Emil, E., Alkan, G., Gurmen, S., Rudolf, R., Jenko, D., and Friedrich, B. (2018). Tuning the Morphology of ZnO Nanostructures with the Ultrasonic Spray Pyrolysis Process. *Metals* 8, 569. doi:10.3390/met8080569
- Fan, L., Tu, Z., and Chan, S. H. (2021). Recent Development of Hydrogen and Fuel Cell Technologies: A Review. *Energy Rep.* 7, 8421–8446. doi:10.1016/j.egy.2021.08.003
- Fang, Y.-H., and Liu, Z.-P. (2014). Tafel Kinetics of Electrocatalytic Reactions: From Experiment to First-Principles. *ACS Catal.* 4, 4364–4376. doi:10.1021/cs501312v
- Feng, Y., Wang, R., Dong, P., Wang, X., Feng, W., Chen, J., et al. (2021). Enhanced Electrocatalytic Activity of Nickel Cobalt Phosphide Nanoparticles Anchored on Porous N-Doped Fullerene Nanorod for Efficient Overall Water Splitting. *ACS Appl. Mat. Interfaces* 13, 48949–48961. doi:10.1021/acsami.1c16546
- Feng, W., Feng, Y., Chen, J., Wang, H., Hu, Y., Luo, T., et al. (2022). Interfacial Electronic Engineering of Ru/FeRu Nanoparticles as Efficient Trifunctional Electrocatalyst for Overall Water Splitting and Zn-Air Battery. *Chem. Eng. J.* 437, 135456. doi:10.1016/j.cej.2022.135456

- Feng, Y., Feng, W., Wan, J., Chen, J., Wang, H., Li, S., et al. (2022). Spherical vs. Planar: Steering the Electronic Communication between Ru Nanoparticle and Single Atom to Boost the Electrochemical Hydrogen Evolution Activity Both in Acid and Alkaline. *Appl. Catal. B Environ.* 307, 121193. doi:10.1016/j.apcatb.2022.121193
- Fernandes, R., Chunduri, A., Gupta, S., Kadrekar, R., Arya, A., Miotello, A., et al. (2020). Exploring the Hydrogen Evolution Capabilities of Earth-Abundant Ternary Metal Borides for Neutral and Alkaline Water-Splitting. *Electrochim. Acta* 354, 136738. doi:10.1016/j.electacta.2020.136738
- Gupta, S., Patel, N., Miotello, A., and Kothari, D. C. (2015). Cobalt-Boride: An Efficient and Robust Electrocatalyst for Hydrogen Evolution Reaction. *J. Power Sources* 279, 620–625. doi:10.1016/j.jpowsour.2015.01.009
- Gupta, S., Patel, M. K., Miotello, A., and Patel, N. (2020). Metal Boride-Based Catalysts for Electrochemical Water-Splitting: A Review. *Adv. Funct. Mat.* 30, 1906481. doi:10.1002/adfm.201906481
- Hu, C., and Dai, L. (2016). Carbon-Based Metal-free Catalysts for Electrocatalysis beyond the ORR. *Angew. Chem. Int. Ed.* 55, 11736–11758. doi:10.1002/anie.201509982
- Hydrogen Roadmap Europe (2019). *A Sustainable Pathway for the European Energy Transition*. report.
- Jagiello, J., Castro-Gutiérrez, J., Canevesi, R. L. S., Celzard, A., and Fierro, V. (2021). Comprehensive Analysis of Hierarchical Porous Carbons Using a Dual-Shape 2D-NLDFT Model with an Adjustable Slit-Cylinder Pore Shape Boundary. *ACS Appl. Mat. Interfaces* 13, 49472–49481. doi:10.1021/acsmi.1c13910
- Jiang, B., Song, H., Kang, Y., Wang, S., Wang, Q., Zhou, X., et al. (2020). A Mesoporous Non-precious Metal Boride System: Synthesis of Mesoporous Cobalt Boride by Strictly Controlled Chemical Reduction. *Chem. Sci.* 11, 791–796. doi:10.1039/c9sc04498a
- Jones, F., Tran, H., Lindberg, D., Zhao, L., and Hupa, M. (2013). Thermal Stability of Zinc Compounds. *Energy Fuels* 27, 5663–5669. doi:10.1021/ef400505u
- Li, H., Chen, X., Wang, M., and Xu, Y. (2002). Selective Hydrogenation of Cinnamaldehyde to Cinnamyl Alcohol over an Ultrafine Co-B Amorphous Alloy Catalyst. *Appl. Catal. A General* 225, 117–130. doi:10.1016/s0926-860x(01)00855-9
- Li, Y., Jiang, X., Tang, M., Zheng, Q., Huo, Y., Xie, F., et al. (2020). A High-Performance Oxygen Evolution Electrocatalyst Based on Partially Amorphous Bimetallic Cobalt Iron Boride Nanosheet. *Int. J. Hydro. Energy* 45, 28586–28597. doi:10.1016/j.ijhydene.2020.07.140
- Liang, Y.-C., and Wang, C.-C. (2018). Surface Crystal Feature-dependent Photoactivity of ZnO-ZnS Composite Rods via Hydrothermal Sulfidation. *RSC Adv.* 8, 5063–5070. doi:10.1039/c7ra13061a
- Masa, J., Weide, P., Peeters, D., Sinev, I., Xia, W., Sun, Z., et al. (2016). Amorphous Cobalt Boride (Co₂B) as a Highly Efficient Nonprecious Catalyst for Electrochemical Water Splitting: Oxygen and Hydrogen Evolution. *Adv. Energy Mat.* 6, 1502313. doi:10.1002/aenm.201502313
- Murthy, A. P., Madhavan, J., and Murugan, K. (2018). Recent Advances in Hydrogen Evolution Reaction Catalysts on Carbon/carbon-Based Supports in Acid Media. *J. Power Sources* 398, 9–26. doi:10.1016/j.jpowsour.2018.07.040
- Nemiwal, M., Zhang, T. C., and Kumar, D. (2021). Graphene-based Electrocatalysts: Hydrogen Evolution Reactions and Overall Water Splitting. *Int. J. Hydro. Energy* 46, 21401–21418. doi:10.1016/j.ijhydene.2021.04.008
- Pu, Z., Liu, T., Zhang, G., Liu, X., Gauthier, M. A., Chen, Z., et al. (2021). Nanostructured Metal Borides for Energy-Related Electrocatalysis: Recent Progress, Challenges, and Perspectives. *Small Methods* 5, 2100699. doi:10.1002/smt.202100699
- Qiang, C., Zhang, L., He, H., Liu, Y., Zhao, Y., Sheng, T., et al. (2021). Efficient Electrocatalytic Water Splitting by Bimetallic Cobalt Iron Boride Nanoparticles with Controlled Electronic Structure. *J. Colloid Interface Sci.* 604, 650–659. doi:10.1016/j.jcis.2021.07.024
- Singla, M. K., Nijhawan, P., and Oberoi, A. S. (2021). Hydrogen Fuel and Fuel Cell Technology for Cleaner Future: a Review. *Environ. Sci. Pollut. Res.* 28, 12607–15626. doi:10.1007/s11356-020-12231-8
- Siwal, S. S., Yang, W., and Zhang, Q. (2020). Recent Progress of Precious-metal-free Electrocatalysts for Efficient Water Oxidation in Acidic Media. *J. Energy Chem.* 51, 113–133. doi:10.1016/j.jechem.2020.03.079
- Sukanya, R., and Chen, S.-M. (2020). Amorphous Cobalt Boride Nanosheets Anchored Surface-Functionalized Carbon Nanofiber: An Bifunctional and Efficient Catalyst for Electrochemical Sensing and Oxygen Evolution Reaction. *J. Colloid Interface Sci.* 580, 318–331. doi:10.1016/j.jcis.2020.07.037
- Sun, J., Zhang, W., Wang, S., Ren, Y., Liu, Q., Sun, Y., et al. (2019). Ni-Co-B Nanosheets Coupled with Reduced Graphene Oxide towards Enhanced Electrochemical Oxygen Evolution. *J. Alloys Compd.* 776, 511–518. doi:10.1016/j.jallcom.2018.10.296
- Tan, T., Han, P., Cong, H., Cheng, G., and Luo, W. (2019). An Amorphous Cobalt Borate Nanosheet-Coated Cobalt Boride Hybrid for Highly Efficient Alkaline Water Oxidation Reaction. *ACS Sustain. Chem. Eng.* 7, 5620–5625. doi:10.1021/acssuschemeng.9b00258
- Thomas, J. M., Edwards, P. P., Dobson, P. J., and Owen, G. P. (2020). Decarbonising Energy: The Developing International Activity in Hydrogen Technologies and Fuel Cells. *J. Energy Chem.* 51, 405–415. doi:10.1016/j.jechem.2020.03.087
- Wang, Y. D., Ai, X. P., Cao, Y. L., and Yang, H. X. (2004). Exceptional Electrochemical Activities of Amorphous Fe-B and Co-B Alloy Powders Used as High Capacity Anode Materials. *Electrochem. Commun.* 6, 780–784. doi:10.1016/j.elecom.2004.06.002
- Wang, J., Yue, X., Yang, Y., Sirisomboonchai, S., Wang, P., Ma, X., et al. (2020). Earth-abundant Transition-Metal-Based Bifunctional Catalysts for Overall Electrochemical Water Splitting: A Review. *J. Alloys Compd.* 819, 153346. doi:10.1016/j.jallcom.2019.153346
- Wang, P., Chen, B., Li, R., Wang, S., Ren, N., Li, Y., et al. (2021). Cobalt Chloride Hexahydrate Assisted in Reducing Energy Loss in Perovskite Solar Cells with Record Open-Circuit Voltage of 1.20 V. *ACS Energy Lett.* 6, 2121–2128. doi:10.1021/acsenerylett.1c00443
- Wu, L., Li, Q., Wu, C. H., Zhu, H., Mendoza-García, A., Shen, B., et al. (2015). Stable Cobalt Nanoparticles and Their Monolayer Array as an Efficient Electrocatalyst for Oxygen Evolution Reaction. *J. Am. Chem. Soc.* 137, 7071–7074. doi:10.1021/jacs.5b04142
- Wu, H., Feng, C., Zhang, L., Zhang, J., and Wilkinson, D. P. (2021). Non-noble Metal Electrocatalysts for the Hydrogen Evolution Reaction in Water Electrolysis. *Electrochem. Energy Rev.* 4, 473–507. doi:10.1007/s41918-020-00086-z
- Xu, N., Cao, G., Chen, Z., Kang, Q., Dai, H., and Wang, P. (2017). Cobalt Nickel Boride as an Active Electrocatalyst for Water Splitting. *J. Mat. Chem. A* 5, 12379–12384. doi:10.1039/c7ta02644g
- Yao, Y., Zhang, Z., and Jiao, L. (2021). Development Strategies in Transition Metal Borides for Electrochemical Water Splitting. *Energy Environ. Mater.* In press. doi:10.1002/eem2.12198
- Yu, P., Wang, F., Shifa, T. A., Zhan, X., Lou, X., Xia, F., et al. (2019). Earth Abundant Materials beyond Transition Metal Dichalcogenides: A Focus on Electrocatalyzing Hydrogen Evolution Reaction. *Nano Energy* 58, 244–276. doi:10.1016/j.nanoen.2019.01.017
- Zhang, Q., Zhao, J., Wu, Y., Li, J., Jin, H., Zhao, S., et al. (2020). Rapid and Controllable Synthesis of Nanocrystallized Nickel-Cobalt Boride Electrode Materials via a Microimpinging Stream Reaction for High Performance Supercapacitors. *Small* 16, 2003342. doi:10.1002/sml.202003342
- Zhao, S., Xu, S., Yao, J., Chen, N., Gong, Y., Zhang, X., et al. (2022). Elucidating the Reaction Pathway of Crystalline Multi-Metal Borides for Highly Efficient Oxygen-Evolving Electrocatalysts. *J. Mat. Chem. A* 10, 1569–1578. doi:10.1039/d1ta09078j
- Zhou, Y., and Fan, H. J. (2021). Progress and Challenge of Amorphous Catalysts for Electrochemical Water Splitting. *ACS Mater. Lett.* 3, 136–147. doi:10.1021/acsmaterlett.0c00502
- Zhou, D., Li, P., Xu, W., Jawaid, S., Mohammed-Ibrahim, J., Liu, W., et al. (2020). Recent Advances in Non-Precious Metal-Based Electrodes for Alkaline Water Electrolysis. *ChemNanoMat* 6, 336–355. doi:10.1002/cnma.202000010

Conflict of Interest: The authors declare that the research was conducted in the absence of any commercial or financial relationships that could be construed as a potential conflict of interest.

Publisher's Note: All claims expressed in this article are solely those of the authors and do not necessarily represent those of their affiliated organizations, or those of the publisher, the editors and the reviewers. Any product that may be evaluated in this article, or claim that may be made by its manufacturer, is not guaranteed or endorsed by the publisher.

Copyright © 2022 Quílez-Bermejo, García-Dalí, Karthik, Canevesi, Izquierdo, Emo, Celzard and Fierro. This is an open-access article distributed under the terms of the Creative Commons Attribution License (CC BY). The use, distribution or reproduction in other forums is permitted, provided the original author(s) and the copyright owner(s) are credited and that the original publication in this journal is cited, in accordance with accepted academic practice. No use, distribution or reproduction is permitted which does not comply with these terms.